SURFACE MICROHYDROLOGY DRIVES SELF-ORGANIZED VEGETATION PATTERNING IN SEMIARID GRASSLANDS

A Thesis

Presented to

The Faculty of the Environmental Program

The Colorado College

In Partial Fulfillment of the Requirements for the Degree

Bachelor of Arts in Environmental Science

By

Jordan Cosgrove

May 2024

_____

Dr. Miro Kummel

Professor of Environmental Science, Colorado College

_____

Dr. Charlotte G. Gabrielsen

Assistant Professor of Environmental Science, Colorado College

Abstract

Arid grasslands can self-organize into periodic patterns of vegetated groves and bare intergroves via positive feedback where vegetation increases local infiltration rate coupled with feedback where groves deplete downslope sheet flow, creating stripes of bare ground. This study investigated the shift from homogenous to patterned vegetation in its early stages of development in a short grass steppe in South Central CO due to a precipitation change and the recent emergence of period patches. To understand the mechanics behind this transition, we studied patterns in grass mortality, surface and soil properties, and the spatial relationships between these variables, water and sediment transport, and grass health. Intergroves were found to have a higher and smoother slope than groves. There were significant differences in deep soil properties across groups, with the highest mean bulk density in intergroves and the highest mean water content in interstitial pools. Spatial analysis in ArcGIS showed increasing maximum NDVI with vegetation and decreasing maximum NDVI with intergrove cover, as well as decreasing maximum NDVI with distance from interstitial pools, and vegetation and interstitial pool cover significantly predicted maximum NDVI. Because the residuals are autocorrelated, we proceeded with spatial lag models which suggested strong autocorrelation of error and a neighborhood impact of NDVI on itself. The results suggest that with sheet flow, sediment is eroded from intergroves and deposited in groves, forming a stepped horizontal profile. Runoff collects and infiltrates in interstitial pools, redistributing additional water to the grove. Thus, the emerging self-organization improves community water use efficiency, increasing the system's resilience to drought in the face of climate change.

Keywords: periodic vegetation patterns, blue grama, infiltration, sediment transport, arid grasslands, facilitation, microtopography, feedback

Introduction

Periodic vegetation patterns have frequently been observed as a remarkable characteristic of arid and semiarid grasslands. These patterns consist of alternating barren and vegetated patches. It is widely accepted that semiarid communities self-organize into a patterned landscape to more effectively utilize water as a limited resource; however, the connections to other physical and biological drivers at play are not fully understood (Rietkerk et al. 2004; Dunkerley 2018; Valentin et al. 1999). As a result of self-organization, the patterned system is better adjusted to a "stressful" environment and thus more resilient to future disturbance (Rietkerk and van de Koppel 2008).

It is also hypothesized that periodic vegetation patterns are a precursor to more dramatic ecosystem shifts like desertification (Rietkerk et al. 2004; Kéfi et al. 2016). Through this lens, we can consider the development of periodic vegetation patterns to be an early warning sign of "catastrophic regime change" to a homogenous bare state (Rietkerk et al. 2004; Rietkerk and van de Koppel 2008; Kéfi et al. 2016). At the same time, the modification of the physical environment by vegetation is an extraordinary example of resilience, and great care should be taken to understand the mechanisms by which community self-organization is ameliorating the resource distribution question and preventing ecosystem collapse.

Several hypotheses on the driving mechanism behind band formation in semiarid ecosystems have been put forth. Sherratt (2015) observed that vegetation colonized bare ground in patches at their field site in the Sahel. Mabbutt and Fanning (1987) postulated that spatially heterogenous soil properties drove varying vegetation densities at their field site in western Australia. Leprun (1999) suggested that aeolian processes played a critical role in Mali and in Burkina Faso. Tongway and Ludwig (1990) highlighted sediment transport associated with the

hydrological regime as a key process. However, there is a consensus as reviewed by Dunkerley (2002) that overland flow and infiltration rates are fundamental drivers. Importantly, all discourse to date stems from studies on mature periodic vegetation patterns, so researchers can only hypothesize on the original unpatterned state.

Several conditions must be met for an arid or semiarid grassland to undergo periodic vegetation pattern formation. Firstly, the ecosystem must receive between 60 and 500 mm of precipitation annually (Noy-Meir 1973), making water a strong limiting resource in biomass production. It is characteristic of these systems to receive variable and infrequent rainfall events, so the relatively dormant system must be able to respond efficiently to pulses in water availability (Noy-Meir 1973). Because water is both scarce and unpredictable, contiguous vegetation cover cannot be sustained, and thus self-organization facilitates the survival of periodically spaced vegetated patches by local concentration of water (Dunkerley 2018).

For periodic vegetation patterning to occur, the ecosystem must also have a gradual slope of about 1% (Bromley et al. 1997) and contain low infiltrability soils susceptible to surface crusting (Valentin et al. 1999). These two conditions are necessary to produce uniform overland flow, or sheet flow, during significant rainfall events which drives water redistribution through the system. Sheet flow transports water from bare patches with low infiltrability to vegetated groves oriented perpendicular to hillslope, defining a runoff and run-on system. In groves, vegetation density induces high infiltration rates and concentrates additional water and nutrients, creating positive water-biomass feedback (Tongway and Ludwig 1990; Puigdefábregas 2005; Meron 2019). At the same time, the depletion of water in the associated intergroves and their limited vegetative success drives surface crusting, increasing soil bulk density, and decreasing soil water content through the same water-biomass feedback (Dunkerley 2018; Dunkerley 2002).

Sheet flow also enables surface sediment transport dynamics. Tongway and Ludwig (1990) describe intergroves as erosional zones and groves as interception or depositional zones. As a result of this patterned redistribution of surface sediments, a grove-intergrove system such as that observed in ecosystems with periodic vegetation patterning can organize into "steps" where the grove exhibits a low angle slope in comparison to the steep intergrove where sediment has been stripped away (Tongway and Ludwig 1990). However, this is not always the case. Dunkerley and Brown (1999) observed a concave upwards topographic profile in which intergroves were situated on a relatively low angle slope, followed by a depositional scarp and a steep grove, which was also modeled by Saco et al. (2007). This suggests that the erosional-depositional dynamics differ between systems, which can be explained by vegetative makeup, soil properties, or developmental stage.

Biological and physical mechanisms interact at different scales to produce short-distance facilitation of vegetation health within groves and simultaneous long-distance inhibition between a grove and an adjacent downslope intergrove. The positive water-biomass feedback acts at a small scale but depletes water at a larger scale, causing competition for a limited resource between groves (Kéfi et al. 2016; Rietkerk and van de Koppel 2008; Meron 2019). Rietkerk and van de Koppel (2008) describe this process as scale-dependent feedback that can create periodic vegetation patterns from an originally homogenous system. Both the facilitative and inhibitive feedbacks, tightly coupled in their dependence on water as a controlling resource, must have associated spatial extents for strong regularity to arise (Rietkerk and van de Koppel 2008; Kéfi et al. 2007). Theoretical literature suggests that both feedbacks are sufficient and necessary to model periodic vegetation pattern formation at a fundamental level (Kéfi et al. 2007).

While mature periodic vegetation patterns appear frequently in scientific discourse,

studies on band development as it is observed in its early stages are rare. Valentin et al. (1999) suggest that as of the end of the 20th century, emerging systems were uncommon due to the specific soil properties, slope gradient, and precipitation regime preconditions for pattern establishment. However, it is possible that instances of pattern development are becoming more common in the wake of climate change, as exemplified by our study site in which periodic vegetation patterns are developing before us.

Our study site provides a unique opportunity to examine periodic vegetation pattern development in the last 25 years out of a mostly homogenous vegetated state (Fig 1). Since the 2000's, our study site has experienced three severe drought years with annual rainfall below 50% of the mean in 2002, 2012, and 2020 (*Colorado Climate Data*). At a study site 30 km south of Chico Basin Ranch, Rondeau et al. measured a 45% decrease in blue grama ground coverage from before to after the 2002 drought, with evidence of slow recovery 7 years post-drought (2013). This finding is consistent with visual assessment of aerial imagery of our study site between 2003 and 2023 showing a significant decrease in grass cover with increased patchiness (Fig 1). Further, a preliminary study of our system by McDonald (2023) documented a shift from anisotropic aperiodic patterning in 2005 to messy but decidedly periodic in nature since 2017. We have continued to observe pattern intensification since then.

The theory of periodic pattern formation cannot be applied without being situated within the context of the site. Our study site is composed predominantly of blue grama, a quintessential drought- and grazing-tolerant perennial bunchgrass of the Central Plains (Smith et al. 2004) whose life history strategy as a bunchgrass is key to the microhydrological dynamics of our system. It thrives on clay and loam soils, with 85% of root mass in the uppermost 20 cm of soil (Smith et al. 2004). Blue grama is a warm-season C_4 grass and is incredibly widespread due to its

ability to rapidly increase leaf water potential and root growth in response to bursts of rainfall (Smith et al. 2004; Lauenroth et al. 1987). As a bunchgrass, blue grama produces hummocks interspersed with bare interstitial spaces. Aguilera and Lauenroth (1993) suggest that plant spacing around these interstitial spaces indicates the depletion of spatially distributed resources. Seedling establishment in these interstitial spaces is also negatively affected by conspecific adult neighbors, supporting the theory of significant belowground competition (Aguilera and Lauenroth 1995). As stand establishment by seed is severely inhibited, blue grama most commonly reproduces by hummock-forming tillering (Smith et al. 2004). As a result, these small unvegetated pockets often prevail and serve as shallow drainage pools during rainfall events, where waterlogging further suppresses blue grama colonization (USDA NRCS Plant Materials Program 2006). At our field site, these interstitial spaces were topographically depressed and the soil surface was crusted and cracked, indicating that they were indeed places of ephemeral ponding (Fig 2b). The intergroves were covered in a loose, dusty sediment, underneath which was a crust that appeared paler and smoother than the interstitial pool crusts (Fig 2a). These preliminary observations suggested that spatial components were at play in the water and sediment transport processes, which further informed our decision to study developing periodic vegetation patterning at this location.

Our study aims to investigate the microhydrological processes associated with band development. Our goal was to analyze the ways in which (1) patchiness originates from a homogenous vegetation cover, (2) water accumulation and vegetation density create positive feedback, (3) sediment transport alters the physical environment, and (4) biological and physical drivers interact at different spatial scales to generate periodic patterning. To answer these questions we studied grove organization, infiltration rates, small-scale topographical variation,

deep soil and surface soil properties, and spatial relationships between grass health and surface cover.

Methods

Site description

Our study site was in a semi-arid short-grass prairie at Chico Basin Ranch in South Central Colorado (38°30'48.23"N, 104°25'20.15"W). Our field site was located directly east of the ranch airstrip on a 60 m by 180 m plot with a gradual 0.8% southeast facing slope, sitting atop Pierre shale. The site receives an average of 300 mm of annual precipitation, most of which falls in thunderstorms from the spring into summer months (*Colorado Climate Data*; Rondeau et al. 2013). The site is dominated by *Bouteloua gracilis* (Blue grama) but also sees *Cylindropuntia imbricata* (Cholla cactus), *Bouteloua dactyloides* (Buffalo grass), and invasive *Salsola tragus* (Russian thistle). Ranch management consists of rotational grazing of cattle, with pastures receiving long rest periods often exceeding one year. We collected all data between September 25, 2023 and October 18, 2023.

Our system is comprised of alternating bands of bare intergroves and vegetated groves oriented parallel to hillslope contours. Dominant wavelengths as analyzed by Fast Fourier Transform are between 15 and 19 m (McDonald 2023). Intergroves range from 8-15 meters across and about 2m wide, and are dispersed throughout a matrix of vegetation, generally about 5-15 m apart (Fig 1). Intergroves consist of little to no live vegetation, but often contain dead blue grama tillers suspended by dead roots above the eroded soil surface (Fig 2a). Groves are vegetated primarily with blue grama (95% of vegetation cover), with Russian thistle, an invasive tumbleweed, occasionally colonizing the upslope edges of groves (<5% of vegetation cover). Mature cholla cacti are randomly dispersed throughout the site.

Ground cover type in the field

We placed 20 transects originating from the middle of an uphill grove, through the intergrove to the middle of the downhill grove at our field site. The transects were placed perpendicular to the bands, intersecting the widest portion of the intergrove. By design, the transects were variable in length; the average transect length was 9.35m. To place the transects we moved in two parallel lines 20 m apart, starting from northern edge of our field site and moving south, and placed a transect at every intergrove we encountered until the final count of 20 was reached.

Along each transect, we moved a 0.5 m by 0.5 m survey quadrat in 0.5 m increments, within which we counted 2.5x2.5 cm kernels of senescing grass and of dead grass. Senescing grass maintained dull brown or gray blades, whereas dead grass was defined by a remaining raised structure of leafless exposed abraded tillers perched on dead roots. We also took a photograph of each quadrat for further analysis. We overlaid a grid containing 100 intersection points on the photographs and counted the occurrences of live grass and bare ground to estimate percent coverage. To aggregate these variable-length transects for statistical analyses we standardized them to be of length of 1, with distances along the transects being expressed as fractions of the length.

Microtopography

We collected microtopographic profiles along 11 transects placed downslope and perpendicular to representative grove-intergrove units. A Bosch GOL26 auto level was used to measure the height of a meterstick to the nearest millimeter. The meter stick was held exactly vertically and was moved in 10 cm increments along the transect. For each point we recorded elevation, and surface type: (1) bare ground with fine dust overlying crusted surface typical of

intergroves, (2) bare ground with cracked and peeling crust typical of interstitial pools in the groves, (3) living grass, (4) dead grass.

Each profile was plotted and keyed by surface type to visualize small-scale changes in surface topography. Intergrove soil and grove soil (interstitial pool) segments were extracted from each transect, and their slopes were calculated. Variance of residuals was calculated for each segment as a measure of surface smoothness. A paired t-test was conducted on the slopes of 12 pairs of intergrove and adjacent downslope grove (one transect contained two pairs). A paired t-test was also conducted on the variance of residuals of the 12 pairs.

Infiltration in the field

At 36 representative locations of bare ground, healthy grass hummocks, and large interstitial pools (12 each), we hammered a segment of heavy-duty PVC pipe, 24 cm in diameter with a beveled bottom edge, 1 cm into the ground to prevent lateral spillage. We poured one liter of water into the pipe and measured time to complete infiltration. A one-way ANOVA was performed to test for a difference in infiltration time between groups, followed by a Bonferroni's pairwise comparison of means.

Soil bulk density and soil water content

At 20 grove-intergrove units, we collected a soil core of (1) intergrove soil, (2) soil beneath dead grass in the intergrove, (3) soil beneath interstitial pool in the grove, and (4) soil beneath living grass in the grove. Cores were 15 cm in depth. Each core was weighed, dried at 60 C for 48 hours, and reweighed to the nearest 0.001 g to calculate bulk density and water content (Corbin and Robertson n.d.; Robertson and VanderWulp n.d.). A one-way ANOVA was performed to test for a difference in bulk density between groups, and again for a difference in water content.

Surface sediments

At the same 20 sites, we collected three surface soil samples; (1) loose dust brushed off the intergrove surface, (2) intact pieces of the crust immediately underneath the intergrove dust, and (3) intact pieces of crust from the interstitial pools with characteristic cracking and curled edges.

To conduct particle size analysis and construct a particle size distribution curve, 400g of each soil sample underwent initial sieving through #8, #10, #16, #18, #25, and #40 (1.0, 0.9, 0.63, 0.56, 0.45, and 0.28 mm) sieves, with the percent passing recorded for each sieve by comparing the weight of the empty sieve to the weight of the sieve containing the retained soil particles. The hydrometer method was employed to analyze particles smaller than 0.28 mm that passed through the #40 sieve (Gavlak et al. 2005). 50.00 ±0.05 grams of soil that passed through #40 sieve were added to 100ml of a 5% Sodium Hexametaphosphate (HMP) dispersing solution to ensure effective dispersion during analysis. The slurry was then added to 1000 ml of deionized water. A Standard hydrometer, ASTM No. 1.152H-Type with Bouyoucos scale in g L-1, was utilized to record readings at time intervals of 15 seconds, 30 seconds, 1 minute, 2 minutes, 4 minutes, 8 minutes, 16 minutes, 30 minutes, 1 hour, 2 hours, 4 hours, and 8 hours. These times reflect the observation that sand and silts settle quickly and clay particles settle after 7 hours and 45 minutes (Gavlak et al. 2005). The hydrometer analysis was conducted at a constant temperature of 20°C.

Hydrometer calculations utilized equations derived from Stokes' law to compute particle size and percent fineness. Equations 1 and 2 from Geosystem Support Software (2020) were used to calculate particle size and percent finer,

$$Particle\ size = \sqrt{\frac{30 \times \nu \times L}{980 \times (GS - GW) \times ET}} \quad (1)$$

$$Percent\ finer = Rc \times A \times WB \times 100\% \quad (2)$$

where v is the fluid viscosity in centipoise (0.01005), L is the effective depth in centimeters (L = 16.295 - 0.165*Reading corrected for meniscus), GS is the specific gravity of the soil particles (2.65), GW is the specific gravity of water at 20 degrees Celsius (0.99823), Et is the elapsed time in minutes, Rc is the corrected hydrometer reading, A is the specific gravity of solids (assumed as 1), and WB is the biased hydrometer sample weight (50 g).

Aerial data (digital elevation model and 5-band multispectral orthomosaic)

We flew a UAV mission (DJI Inspire 2 equipped with a MicaSense Altum multispectral drone sensor) to create a 6-band multispectral orthomosaic and digital elevation model (DEM) of the study site. The mission was flown on October 14, 2023, at 11 am during uniformly sunny weather at 13m elevation and in a lawnmower pattern with 85% by 85% overlap. It was processed into a DEM and a 6-band orthomosaic with Agisoft Metashape using 15 ground control points collected with a Trimble Geoexplorer 6000 GPS. After differential correction 100% of the ground control points had estimated accuracy at or below 15cm. The pixel size of the DEM and orthomosaic was 0.56cm by 0.56cm, making blades of grass observable in the orthomosaic. Figure 8a shows a representative grove-intergrove unit from the orthomosaic.

A supervised classification of the 6-band orthomosaic in ArcGIS Pro classified the site into three categories by spectral signature: vegetation, intergrove soil, and grove soil. Classification accuracy was assessed using a confusion matrix and via visual assessment. To identify interstitial pools where water infiltrates within the groves, we interpolated the ground surface without vegetation using the Kriging method on points classified as soil and subtracted the original DEM from this layer. This highlighted spots where elevation was lower than expected (pools) and higher than expected (vegetation). We then identified interstitial pools as

pixels both classified as grove soil and positioned 10 cm below the expected surface. The 10 cm threshold was chosen for its visual correspondence to pool locations based on sediment color and texture.

The multispectral orthomosaic was then used to calculate NDVI,

$$NDVI = \frac{NIR-red}{NIR+red} \quad (3)$$

of the site (Fig 8c). The highest NDVI signatures belonged to cholla and tumbleweed plants, both of which are not representative of the spatial relationships this study attempts to evaluate, so we excluded these cells to best represent blue grama as the ecosystem engineer. We excluded cells by a combination of hand-digitizing, supervised classification, and strong positive divergence from the Kriging ground surface.

The orthomosaic was then split into a grid of 9781 50x50 cm polygons. Each polygon was assigned mean NDVI, maximum NDVI, and percent coverage of vegetation, percent cover by intergrove soil, and percent cover by interstitial pools. NDVI-max was ultimately used to quantify grass health because mean NDVI appeared colinear with percent coverage of vegetation. The shapefile was read into RStudio using the sf package, where we ran Pearson's correlation tests between each type of coverage and NDVI-max.

Spatial statistical analyses

Spatial correlations and adjustment for autocorrelation

Moran's I for NDVI-max, percent vegetation cover, percent intergrove cover, and percent interstitial pool cover were calculated using the spdep package in R. These autocorrelation coefficients were used to adjust the effective sample size in correlation analyses using Equation 4 from Dale and Fortin (2014),

$$Adjusted\ n = n \times \frac{1-\rho_1 \times \rho_2}{1+\rho_1+\rho_2} \quad (4)$$

where n is the original sample size, ρ_1 = Moran's I of variable 1, ρ_2 = Moran's I of variable 2.

Spatial regression

Multiple linear regression of percent interstitial pools and percent vegetation cover was conducted against NDVI-max. Because the residuals of the regression were autocorrelated (Moran's I = 0.1318547), we proceeded with three explicitly spatial models, the Spatial Error Model (SEM), the Spatially Lagged X Model (SLX), and the Spatial Lag Model (SLM) using the spatialreg package in R.

Interstitial pool buffer analysis

We nested a series of 15 buffers around the interstitial pools in 10 cm increments up to 1.5 meters, at which point the surface was almost entirely accounted for. We performed a Pearson's correlation test between buffer distance from the nearest interstitial pool and NDVI-max of the buffer in R.

Results

Patterns of grass mortality

The densities of bare ground, dead grass, and senescing grass exhibit hump-shaped curve when plotted along the standardized transect distance, while the cover of living grass exhibits a "U-shaped" pattern along the standardized transect distance (Fig 3). The peaks of the surface cover types, from upslope to downslope, are in the order of living grass of the uphill grove, senescing grass, dead grass, ground, living grass of the downhill grove. This pattern is consistent with qualitative field observations of the decreasing health of blue grama at the downslope edges of groves.

Comparison of infiltration rates between intergroves, grassy patches, and interstitial pools

Bare intergrove soil had the longest average infiltration time at 18.3 minutes (SD = 17.2),

followed by interstitial pools at 12.8 minutes (SD = 8.8) and grassy patches at 2.6 minutes (SD = 0.77). One-way analysis of means not assuming equal variance gave a significant difference in means between groups ($F(2,18.81) = 12.526$, $p < 0.001$). A Bonferroni's pairwise comparison gave a significant difference in means between grassy patches and interstitial pools ($p < 0.01$) and between grassy patches and bare intergrove soil ($p < 0.05$).

Comparison of topographical slopes and roughness coefficients between groves and intergroves

Plots of microtopographic profiles show visible differences in slope and surface roughness between bare ground points in groves and intergroves (Fig 4). A paired t-test between grove and intergrove slopes found that intergrove segments had a significantly steeper slope ($t(11) = -3.9982$, $p < 0.01$). The mean slope of intergrove segments was -0.979 cm/m (SD = 0.0923), and the mean slope of grove segments was -0.389 cm/m (SD = 0.1069) (Fig 5a). A paired t-test between the variance of residuals between grove and intergrove segments found higher variability within grove segments ($t(11) = -3.7314$, $p < 0.01$). The mean variance of residuals was 0.109 (SD = 0.01627) for intergroves and 0.482 (SD = 0.109275) for groves (Fig 5b).

Comparison of bulk density and water content

One-way ANOVA was performed on the bulk densities of soil cores by group ($F(3, 75) = 30.33$, $p < 0.001$) followed by a Tukey multiple comparison of means. Intergrove soil had the highest mean bulk density (M = 1.474906 g/cm^3, SD = 0.05069949), followed by dying grass (M = 1.352609 g/cm^3, SD = 0.09910256), depositional pools (M = 1.335281 g/cm^3, SD = 0.07577807), and lastly living grass (M = 1.245159 g/cm^3, SD = 0.06775758) (Fig 6a). All groups were found to have a statistically significant pairwise difference in means ($p < 0.01$) with

the exception of the comparison between depositional pools and dying grass.

We then carried out one-way ANOVA ($F(3, 75) = 22.05$, $p < 0.001$) and Tukey multiple comparison of means on water content of the soil cores. The depositional cores had the highest soil water content (0.07527233 g/cm^3, SD = 0.01259874), followed by intergrove soil (M = 0.05313619, SD = 0.01516728), live grass (M = 0.05012847, SD= 0.01169302), and dead grass (M = 0.04620406, SD = 0.009731161). The depositional cores were significantly different from all other groups ($p < 0.001$) (Fig 6b).

Analysis of surface sediments

Our particle size distribution curves show that depositional pool crust contains the highest proportion of fine particles (< 0.1 mm), followed by intergrove crust. This is clear at the 20% threshold, where < 0.015 mm particles are remaining for depositional crust and < 0.04 mm particles are remaining for intergrove crust and dust. All sample types appear to have comparable amounts of larger particles (0.2 to 1 mm), with intergrove dust exhibiting the highest proportions.

Correlations between surface cover and NDVI-max

We found a positive correlation between grass cover and NDVI-max ($r(9779) = 0.504247$, $p < 0.001$) (Fig 9a) and a negative correlation between intergrove dust coverage and NDVI-max ($r(9779) = -0.368889$, $p < 0.001$) (Fig 9b). Please note that the "NDVI-max" here is an operationalization of vegetation health within the 50x50cm square, whereas average NDVI would be more closely approximating vegetation coverage. Moran's I coefficient of autocorrelation was 0.165323 for NDVI-max 0.2654579 for percent coverage of vegetation, and 0.28854 for percent coverage of intergrove soil, suggesting clustering of each variable. To correct for the autocorrelation, adjusted sample sizes and p-values for the significant correlations

were calculated using Equation 4 (Dale and Fortin 2014). Between NDVI-max and vegetation density, the adjusted sample size decreased from 9781 to 3317.53 ($p<0.001$). Between NDVI-max and intergrove soil, adjusted sample size decreased to 6406.672 ($p<0.001$). Both correlations were significant using the adjusted "effective sample size." There was no significant correlation between interstitial pool cover and NDVI-max ($r(9779)= 0.002350959$, $p > 0.05$) (Fig 9c).

OLS results

Multiple linear regression of NDVI-max as a function of vegetation cover and pool cover was significant ($F(2,9778)=1695$, $p < 0.001$, $R^2 = 0.2574$). Both independent variables explain significant proportions of variability in the dependent variable (β (vegetation density) = 0.098, $p < 0.002$; β (interstitial pool coverage) = 0.042, $p < 0.007$) (Table 1). The global Moran's I for the residuals of the regression was 0.1318547, suggesting a strong autocorrelation of the values of the residuals ($p < 0.001$). Thus, we had sufficient reasoning to proceed with spatial models to better explain the relationship.

Spatial regression results

To assess whether there was a lagged neighborhood impact of vegetation or pools on NDVI, we ran three spatial regressions: a spatial error model (SEM), a spatially lagged x model (SLX), and a spatial lag model (SLM) in R (Table 1) using the spatialreg package in R. The SEM was chosen because it corrects for the autocorrelation of the residual errors, offering insight into the strength with which the explanatory variables are explaining spatial variability. The SEM showed both vegetation and pool cover within a queen (8 neighbor) neighborhood were statistically significant in explaining local NDVI-max with individual beta values virtually unchanged compared to the non-spatial model. However, the residual errors were highly

autocorrelated ($\lambda = 0.34882$, $p<0.001$), suggesting a possible missing explanatory variable in the regression model. The SLX reports both local and neighborhood effects of explanatory variables to uncover the significance of spatial lag in the effects of vegetation cover and interstitial pools on grass health. Because of the positive biomass-water feedback in grove patches, we expected to find spatially lagged effects of the explanatory variables where both local and neighborhood plant densities and pool coverage would contribute to the local vegetation health. However this was not the case: while the model as a whole was statistically significant ($F(4, 9776)=848$, $p<0.001$, $R^2 = 0.2576$), the effects of neighborhood grass cover and neighborhood pool density were not. Lastly, we ran the SLM to find whether local NDVI had a propagating effect on global NDVI. The SLM suggested that there is a spatial effect of the dependent variable, NDVI-max, on itself ($\rho = 0.28175$, $p<0.001$).

Interstitial pool buffer results

A Pearson's correlation test showed decreasing NDVI-max with distance from an interstitial pool, suggesting the healthiest grasses are adjacent to interstitial pools ($r(13) = -0.8074528$, $p < 0.001$) (Fig 10).

Discussion

The periodic vegetation pattern likely developed via spatially aggregated death of grass

Our study site has gone through a dramatic transformation over the past decade, from a fairly homogeneous state in 2003 (Fig 1a) to a distinctly banded state in 2023 (Fig 1b). In a preliminary study conducted at our site, McDonald (2023) identified slight aperiodic anisotropic patchiness in 2003 and significant periodic patterning by 2017, with the transformation towards periodicity attributed to tighter spatial coupling in response to the 2002 and 2012 droughts. In the time since the analyses performed by McDonald (2023) the site experienced another significant

drought in 2020. The observed ecosystem transformation reported in this study is consistent with an assessment by Rondeau et al. (2013) of a significant decrease in grass density at a field site 30 km south in the same ecosystem type over the 1990-2012 timespan. The goal of this study is to examine the role of microhydrology in this transformation.

Our study finds that patchiness and vegetation banding likely results from grass death in distinct bands in response to three severe non-consecutive drought years. In intergroves, dead protruding tillers suspended on brittle dead roots indicate that blue grama previously grew in the bare patches but have since declined. From our vegetation cover transects, we also observed early grass senescence and high occurrences of grass death in the downslope segments of groves (Fig 3). In conjunction with historical aerial imagery from Google Earth (Fig 1a), we can conclude that the site began as fairly homogenous in vegetation density but gained bare patches through processes of en-masse grass mortality. Further, the early senescence of grass at the downslope edges of groves suggests that this process is still occurring as bands continue to develop and periodicity strengthens.

Infiltration rates

Changes in vegetation density have clear effects on local infiltration rates. We observed the highest infiltration rates in the hummocks of blue gramma and significantly lower infiltration rates in the intergroves and interstitial pools within the grass groves. In degraded patches of the intergroves, exposed surface sediments likely become compacted by the percussive action of rainfall on bare soil (Tongway and Ludwig 2001), forming a cement-like compressed crust with high mechanical strength (Dunkerley 2018). Our analysis confirms that in our system, intergrove soil has the highest bulk density. Such dense soils not only limit infiltrability as shown by our infiltration test but make the patch unsuitable for colonization by plants which could contribute

to breaking up the soil surface and increasing infiltrability (Valentin et al. 1999). At the same time, infiltration rates remain high in vegetated groves due to more robust pathways into the ground such as macropores (Greene 1992), cracks in the crust, and the permeative action of grass roots (Meron 2019). This is supported by our analyses of deep soil water content which found a high mean concentration of water underneath interstitial pools long after the most recent rainfall event.

Water redistribution within a grove-intergrove unit

Low infiltration in the intergrove creates runoff into the immediate downslope vegetated grove, where run-on is intercepted and infiltrates more easily. Sheet flow occurs on gentle, uniform slopes of about 1%, where soil surface conditions are susceptible to crusting and thus infiltration rates are low (Bromley et al. 1997; Valentin et al. 1999; Tongway and Ludwig 2001). These preconditions are met in our system, causing rainfall onto the bare patch to be uniformly diverted towards the immediate downslope grove as sheet flow. This intergrove-grove sequence creates a “basic functional unit” in which water is theoretically conserved through the interaction between intergroves as a source and groves as a sink (Tongway and Ludwig 2001; Noy-Meir 1973).

The functioning of the source-sink unit means that groves receive additional water. A grove can hypothetically collect twice the amount of water from run-on as it would from only direct rainfall without the presence of an upslope intergrove (Aguiar and Sala 1999; Valentin and d’Herbès 1999). Thus, even if mean water inputs into the system are too low for homogenously distributed grasses to survive, the concentration of water into groves facilitates vegetative success in those patches (Rietkerk and van de Koppel 2008; Dunkerley 2018). Further, the grove minimizes water loss out of the system compared to non-patterned landscapes by about 8%

(Ludwig et al. 1999), meaning that community water use efficiency is improved by effective absorption and utilization (Tongway and Ludwig 1990). However, runoff is not equally distributed throughout the grove. The downslope edge of the grove receives less water than the upslope edge due to depletion by the upslope edge (Bromley et al. 1997). This is supported in this study by senesced and dead grass density peaks occurring downslope of the live grass density peak, as water is less available.

Water-biomass feedback

A positive feedback loop occurs in the grove between vegetation density, infiltration rate, and water availability. As demonstrated, groves receive supplementary water as runon which infiltrates relatively quickly. This supports vegetation health, which in turn facilitates root growth and bioturbation which further promote infiltration. In addition, groves create a microenvironment that reduces evaporation by shielding the soil from radiation and wind (Noy-Meir 1973; Dunkerley 2018), and they act as "resource islands" in which organic matter is recycled within the system, increasing nutrient availability (Puigdefábregas 2005; Ludwig et al. 1999). Vegetated runon areas had higher levels of soil nitrogen, carbon, and exchangeable cations in a study by Tongway and Ludwig (1990). Ludwig et al. (1999) also showed that systems with bands increase net primary production by 10% compared to patchless landscapes due to their ability to capture nutrients and water. Our study showed that grass health increased with vegetation cover, reflecting the positive impact of grove dynamics on vegetative success. Thus, we can hypothesize that grove success amid drought is likely contingent on preexisting vegetation density and that the development of healthy vegetation bands can largely be attributed to water redistribution from upslope bare patches and nutrient accumulation.

Interstitial pool storage

A key component of within-grove dynamics in our blue gramma system are interstitial spaces (Fig 2b). Sticpewich (2022) showed that surface water depths in interstitial pools in our system remain high long for hours after the water in the intergroves runs off or infiltrates. This long residence time of water in pools drives increased percolation depths and eventual water storage (Sticpewich 2022). Similarly, our analysis of soil water content found that soil underneath interstitial pools acts as water storage long after grasses have depleted local water stores directly beneath the hummocks, indicating that interstitial pools are a key factor in water allocation to groves in the weeks after a rainfall event.

Interestingly, our study found that interstitial pools had infiltration rates comparable to the bare intergroves, suggesting that water is primarily infiltrating laterally through blue grama hummocks and not directly downwards. This is likely, at least in part, due to surface crusting in the interstitial pools. Our sediment particle size distribution analysis showed higher proportions of small particles in interstitial pools (Fig. 7), suggesting that small particles are clogging soil pores as they settle. Because infiltration is slowed, interstitial pools effectively hold water aboveground for lateral infiltration into hummocks where dense roots break up the soil and create belowground pathways through the grove. For these reasons we can hypothesize that diffusion contributes to belowground water storage of interstitial spaces more than direct vertical infiltration.

Spatial effects of vegetation and interstitial pool coverage on NDVI

The results of the SEM show that residual errors within the model are autocorrelated, indicating that adjacent areas share similar NDVI-max beyond what is explained by local vegetation and interstitial pool cover, meaning there is likely a missing explanatory variable in the spatial regression. Soil water content, for example, would be predicted to have a positive

effect on grass health but was not measured systematically through the entire study site. Nonetheless, the SEM indicates that there is indeed a spatial component to the regression. The SLX did not uncover a neighborhood effect of vegetation density and interstitial pool cover on NDVI-max. We expected the water-biomass feedback to occur across a neighborhood scale at which a grove is organized, however our spatial analysis showed that the positive effects of grass coverage on grass health are very centralized. Similarly, the positive effects of pools are also only detectable within 50 cm. This is likely because the water stored underneath interstitial spaces is only accessible to adjacent grasses and not to the entire grove. Lastly, the SLM found lagged effects within the dependent variable, NDVI-max. This means that NDVI-max has a propagating effect on itself at the global scale, which was unexpected.

Erosional-depositional regime

Sediment transport also plays a role in band development by altering the physical system. While aeolian deposits likely exist, we see evidence that most of the sediment transport in our system is runoff driven. The microtopography profiles that we collected showed steep, smooth slopes in intergroves where sediment is eroding away. Thus, our microtopographic transects are indicative of a "stepped" profile with relatively flat groves and steep intergroves (Fig 4 and 5). This finding is not consistent with some previous descriptions of concave up units exhibiting steep groves followed by flatter intergroves and a downslope depositional ridge (Dunkerley and Brown 1999; Saco et al. 2007). Alternatively, Valentin et al. (1999) and Tongway and Ludwig (1990) report that run-off zones are gently sloping into flatter run-on zones, which agrees with this study. Consistent with our understanding of the system, Tongway and Ludwig (1990) attribute their topographic profile to an erosional-depositional regime in which sediment is removed from the bare patches and intercepted by vegetated patches where it is ultimately

deposited. Pickup (1985) refers to this unit as an "erosion cell." Theoretically, just as very little water leaves an intergrove-grove unit, so does sediment. In agreement with Pickup (1985), we hypothesize that the deposition of sediment levels of groves, increasing interceptive capability and thus increasing infiltration rates in positive feedback. At the same time, the bare intergrove is uniformly stripped of surface soils, which increases the speed of overland flow to decrease residence time and infiltration rates. Sediment redistribution into groves, then, can be said to play a role in the success of vegetation in groves.

The initiation of sheet flow plays a critical role in band maintenance, not only because even redistribution of water to groves drives the water-biomass feedback, but because it maintains the smooth, gradual hillslope. Without the necessary slope, rainfall regime, and soil type preconditions, runoff forms channels instead of sheet flow, and a new sediment transport regime gives the landscape rills and gullies, which we did not observe at our study site (Saco et al. 2007). Channel flow does not support band development because of its inability to provide uniform runoff to groves, and likewise the grove's interception of water slows runoff velocity, protecting against rill development. In the absence of vegetated groves, then, the system loses a crucial mechanism in maintaining a physical system that can support vegetation at all. For this reason, severe depletion of vegetation and development of rills and gullies could impair the system's ability to uniformly redistribute runoff, making recovery to periodic vegetation patterning impossible.

Intergroves and interstitial pools exhibit distinct particle size distributions, indicating that sediment transport is preferentially acting on certain sized particles. Our results suggest that when sediment is eroded from bare intergroves, mostly fine particles are picked up and later deposited in interstitial pools. The deposition of fine particles fills in the soil matrix, creating a

surface crust in interstitial pools which decreases local infiltration rates and encourages ponding. Runoff is unable to move large particles, so they are left on the surface of the intergrove. The looseness of dust atop the crust could be attributed to wind-driven transport. Ultimately, our analysis of surface sediment properties between depositional pools and intergroves are consistent with our understanding of the water-driven sediment transport process.

The maintenance of pools by blue grama despite physical alterations of the soil surface by sedimentation is critical in maintaining grove functioning. The upward growth of blue grama hummocks must occur at a similar rate of pool sedimentation to avoid the gradual filling in of pools. In addition, blue grama does not easily establish in interstitial spaces due to resource depletion and conspecific competition (Aguilera and Lauenroth 1993; 1994). These two processes preserve the structure of deep pools, mitigating the loss of the groves' critical water retention mechanism.

Spatially dependent facilitation and competition

Periodic patterning occurs from originally environmentally homogenous systems by facilitation and inhibition of grass health on different spatial scales (Rietkerk and van de Koppel 2008). At a short distance, the grove supports grass health through the positive feedback between vegetation density, community water use efficiency, and nutrient accumulation. At a distinctly longer distance, grass survival in the intergrove is constrained by the associated grove's resource usage. More specifically, the survival of a plant is positively impacted by lateral and downslope plants and negatively impacted by upslope plants due to their role in water redistribution (Valentin et al. 1999). Because small-scale facilitation and large-scale competition each act on different spatial scales, the result is clustering of vegetation in groves directly downslope of bare patches. These two pieces are tightly coupled due to the runoff-run-on regime within an

intergrove-grove unit.

Because these spatially distinct feedbacks are interrelated with water redistribution, the intergrove-grove width ratio can be explained as a function of water availability. Valentin and d'Herbès (1999) found that decreased mean annual rainfall was correlated with increased intergrove-grove width ratio. So, the level of biomass that can be sustained is a function of mean annual precipitation (Valentin et al. 1999). Water scarcity amplifies the long-distance negative feedback, causing bare intergroves to widen. This is because less vegetation can be supported under that precipitation regime, so more intergrove is required to reallocate increased runoff to groves. In our system, stripes of dead and senescing grass downslope of healthy grass suggest that intergroves are indeed widening as they develop.

Periodic vegetation pattern development as a warning sign of regime shift

Widening intergroves introduce the possibility of a catastrophic regime change. In a bistable system, two stable states are possible under the same conditions. At different levels of precipitation in our semiarid system, different stable states include homogenous vegetation to gapped, striped, spotted, and eventually homogenously bare (Meron 2019). A critical decrease in vegetative success or precipitation has the potential to initiate a transition to a homogenously bare state (Rietkerk and van de Koppel 1997; Rietkerk et al. 2004; Karssenberg et al. 2017), wholly eliminating the positive water-biomass feedback altogether. It is hypothesized by Rietkerk et al. (2004) that periodic vegetation patterning, then, is an early warning sign of desertification. In the case that the system contains a catastrophic bifurcation, returning to a vegetated state is unlikely in the context of increasing drought events with climate change. Alternatively, Kéfi et al. (2007; 2013) assert that an ecosystem can undergo "slowing down," without catastrophic regime change. In either case, self-organization into periodic vegetation

patterns enables persistence at lower levels of precipitation than a continuously vegetated state would (van de Koppel and Rietkerk 2004; Dunkerley 2018), increasing community resilience to water scarcity and protecting from a theoretical catastrophic regime shift.

Conclusion

The findings of this study suggest that biological and physical mechanisms are tightly coupled in band development due to their relationship to water availability and transportation. The water-biomass feedback within groves facilitates grass survival at a short distance while water depletion inhibits survival at a larger scale, creating a spatially patterned landscape. At the same time, the movement of water through the system drives sediment transport, altering the microtopography and intensifying water-dependent feedbacks. As a result, an increase in water scarcity could disrupt the stable patterned state and drive a regime shift to an unpatterned, homogenously bare landscape. Indeed, severe drought events are becoming more common with climate change, making understanding semiarid systems even more pressing with the possibility of catastrophic regime changes around the corner.

References

Aguiar, M. R., & Sala, O. E. (1999). Patch structure, dynamics and implications for the functioning of arid ecosystems. *Trends in Ecology & Evolution*, *14*(7), 273–277. https://doi.org/10.1016/S0169-5347(99)01612-2

Aguilera, M. O., & Lauenroth, W. K. (1993). Neighborhood Interactions in a Natural Population of the Perennial Bunchgrass Bouteloua gracilis. *Oecologia*, *94*(4), 595–602.

Aguilera, M. O., & Lauenroth, W. K. (1995). Influence of Gap Disturbances and Type of Microsites on Seedling Establishment in Bouteloua Gracilis. *Journal of Ecology*, *83*(1), 87–97. https://doi.org/10.2307/2261153

Bivand, R., Altman, M., Anselin, L., Assunção, R., Bera, A., Berke, O., Blanchet, F. G., Carvalho, M., Christensen, B., Chun, Y., Dormann, C., Dray, S., Dunnington, D., Gómez-Rubio, V., Koley, M., Krainski, E., Legendre, P., Lewin-Koh, N., Li, A., … Yu, D. (2024). *spdep: Spatial Dependence: Weighting Schemes, Statistics* (1.3-3) [Computer software]. https://cran.r-project.org/web/packages/spdep/index.html

Bivand, R., Piras, G., Anselin, L., Bernat, A., Blankmeyer, E., Chun, Y., Gómez-Rubio, V., Griffith, D., Gubri, M., Halbersma, R., LeSage, J., Li, A., Li, H., Ma, J., Mallik, A., Millo, G., Pace, K., Peres-Neto, P., Rüttenauer, T., … Tiefelsdorf, M. (2024). *spatialreg: Spatial Regression Analysis* (1.3-2) [Computer software]. https://cran.r-project.org/web/packages/spatialreg/index.html

Bromley, J., Brouwer, J., Barker, A. P., Gaze, S. R., & Valentine, C. (1997). The role of surface water redistribution in an area of patterned vegetation in a semi-arid environment, south-west Niger. *Journal of Hydrology*, *198*(1), 1–29. https://doi.org/10.1016/S0022-1694(96)03322-7

Colorado Climate Data, Pueblo Memorial Airport. (n.d.). [dataset]. Colorado State University's

Colorado Climate Center. Retrieved April 16, 2024, from https://climate.colostate.edu/data_access_new.html

Corbin, D., & Robertson, P. (n.d.). *Soil Bulk Density—Deep Cores*. Kellogg Biological Station Long-Term Ecological Research. Retrieved March 12, 2024, from https://lter.kbs.msu.edu/protocols/110

Dale, M. R. T., & Fortin, M.-J. (2014). *Spatial Analysis; A Guide for Ecologists* (2nd ed.). Cambridge University Press.

Deblauwe, V., Barbier, N., Couteron, P., Lejeune, O., & Bogaert, J. (2008). The global biogeography of semi-arid periodic vegetation patterns. *Global Ecology and Biogeography*, *17*(6), 715–723. https://doi.org/10.1111/j.1466-8238.2008.00413.x

Deblauwe, V., Couteron, P., Bogaert, J., & Barbier, N. (2012). Determinants and dynamics of banded vegetation pattern migration in arid climates. *Ecological Monographs*, *82*(1), 3–21. https://doi.org/10.1890/11-0362.1

Dunkerley, D. (2002). Systematic variation of soil infiltration rates within and between the components of the vegetation mosaic in an Australian desert landscape. *Hydrological Processes*, *16*(1), 119–131. https://doi.org/10.1002/hyp.357

Dunkerley, D. (2018). Banded vegetation in some Australian semi-arid landscapes: 20 years of field observations to support the development andevaluation of numerical models of vegetation pattern evolution. *Desert (2008-0875)*, *23*(2), 165–187.

Dunkerley, D. L., & Brown, K. J. (1999). Banded vegetation near Broken Hill, Australia: Significance of surface roughness and soil physical properties. *CATENA*, *37*(1), 75–88. https://doi.org/10.1016/S0341-8162(98)00056-3

Gavlak, R., D. Horneck, and R. Miller. (2005). Plant, soil and water reference methods for the

Western Region. Western Regional Extension Publication (WREP) 125, WERA-103 Technical Committee, http://www.naptprogram.org/files/napt/western-states-method-manual-2005.pdf.

Geosystem Support Software, Inc. (2020). Grain Size Distribution Documentation of Calculations. Retrieved from http://geosystemsoftware.com/support.htm

Greene, R. S. B. (1992). Soil physical properties of three geomorphic zones in a semiarid mulga woodland. *Soil Research*, *30*(1), 55–69. https://doi.org/10.1071/sr9920055

Hlavac, M. (2022). *stargazer: Well-Formatted Regression and Summary Statistics Tables* (5.2.3) [Computer software]. https://cran.r-project.org/web/packages/stargazer/index.html

Karssenberg, D., Bierkens, M. F. P., & Rietkerk, M. (2017). Catastrophic Shifts in Semiarid Vegetation-Soil Systems May Unfold Rapidly or Slowly. *The American Naturalist*, *190*(6), E145–E155.

Kéfi, S., Dakos, V., Scheffer, M., Van Nes, E. H., & Rietkerk, M. (2013). Early warning signals also precede non-catastrophic transitions. *Oikos*, *122*(5), 641–648. https://doi.org/10.1111/j.1600-0706.2012.20838.x

Kéfi, S., Holmgren, M., & Scheffer, M. (2016). When can positive interactions cause alternative stable states in ecosystems? *Functional Ecology*, *30*(1), 88–97. https://doi.org/10.1111/1365-2435.12601

Kefi, S., Rietkerk, M., van Baalen, M., & Loreau, M. (2007). Local facilitation, bistability and transitions in arid ecosystems. *THEORETICAL POPULATION BIOLOGY*, *71*(3), 367–379. https://doi.org/10.1016/j.tpb.2006.09.003

Lauenroth, W. K., Sala, O. E., Milchunas, D. G., & Lathrop, R. W. (1987). Root Dynamics of Bouteloua gracilis During Short-Term Recovery from Drought. *Functional Ecology*, *1*(2), 117–124. https://doi.org/10.2307/2389714

Leprun, J. C. (1999). The influences of ecological factors on tiger bush and dotted bush patterns along a gradient from Mali to northern Burkina Faso. *CATENA*, *37*(1), 25–44. https://doi.org/10.1016/S0341-8162(98)00054-X

Ludwig, J. A., Tongway, D. J., & Marsden, S. G. (1999). Stripes, strands or stipples: Modelling the influence of three landscape banding patterns on resource capture and productivity in semi-arid woodlands, Australia. *CATENA*, *37*(1), 257–273. https://doi.org/10.1016/S0341-8162(98)00067-8

Mabbutt, J. A., & Fanning, P. C. (1987). Vegetation banding in arid Western Australia. *Journal of Arid Environments*, *12*(1), 41–59. https://doi.org/10.1016/S0140-1963(18)31198-4

McDonald, A. (2023). *Desertification in Arid Colorado Shortgrass Steppe? Fast Fourier Transform and Autocorrelation Function Analysis of Emerging Periodic Vegetation Patterns* [Colorado College]. https://digitalcc.coloradocollege.edu/record/3939?ln=en&p=amelia+mcdonald&v=pdf

Meron, E. (2019). Vegetation pattern formation: The mechanisms behind the forms. *Physics Today*, *72*(11), 30–36. https://doi.org/10.1063/PT.3.4340

Noy-Meir, I. (1973). Desert Ecosystems: Environment and Producers. *Annual Review of Ecology and Systematics*, *4*(1), 25–51. https://doi.org/10.1146/annurev.es.04.110173.000325

Particle Size Analysis – Hydrometer Method. (n.d.). Kellogg Biological Station Long-Term Ecological Research. Retrieved March 12, 2024, from https://lter.kbs.msu.edu/protocols/108

Pebesma, E., Bivand, R., Racine, E., Sumner, M., Cook, I., Keitt, T., Lovelace, R., Wickham, H., Ooms, J., Müller, K., Pedersen, T. L., Baston, D., & Dunnington, D. (2024). *sf: Simple Features for R* (1.0-16) [Computer software]. https://cran.r-project.org/web/packages/sf/index.html

Pickup, G. (1985). The erosion cell—A geomorphic approach to landscape classification in range assessment. *Australian Rangeland Journal*, *7*(2), 114–121.

Puigdefábregas, J. (2005). The role of vegetation patterns in structuring runoff and sediment fluxes in drylands. *Earth Surface Processes and Landforms*, *30*(2), 133–147. https://doi.org/10.1002/esp.1181

Rietkerk, M., Dekker, S. C., de Ruiter, P. C., & van de Koppel, J. (2004). Self-Organized Patchiness and Catastrophic Shifts in Ecosystems. *Science*, *305*(5692), 1926–1929.

Rietkerk, M., & van de Koppel, J. (1997). Alternate Stable States and Threshold Effects in Semi-Arid Grazing Systems. *Oikos*, *79*(1), 69–76. https://doi.org/10.2307/3546091

Rietkerk, M., & van de Koppel, J. (2008). Regular pattern formation in real ecosystems. *Trends in Ecology & Evolution*, *23*(3), 169–175. https://doi.org/10.1016/j.tree.2007.10.013

Robertson, P., & VanderWulp, S. (n.d.). *Soil Moisture – Gravimetric*. Kellogg Biological Station Long-Term Ecological Research. Retrieved April 16, 2024, from https://lter.kbs.msu.edu/protocols/24

Rondeau, R. J., Pearson, K. T., & Kelso, S. (2013). Vegetation Response in a Colorado Grassland-shrub Community to Extreme Drought: 1999—2010. *American Midland Naturalist*, *170*(1), 14–25.

Saco, P. M., Willgoose, G. R., & Hancock, G. R. (2007). Eco-geomorphology of banded vegetation patterns in arid and semi-arid regions. *Hydrology & Earth System Sciences*, *11*(6), 1717–1730. https://doi.org/10.5194/hess-11-1717-2007

Sherratt, J. A. (2015). Using wavelength and slope to infer the historical origin of semiarid vegetation bands. *Proceedings of the National Academy of Sciences of the United States of America*, *112*(14), 4202–4207.

Shukla, T., Tang, W., Trettin, C. C., Chen, G., Chen, S., & Allan, C. (2023). Quantification of Microtopography in Natural Ecosystems Using Close-Range Remote Sensing. *Remote Sensing*,

15(9), 2387. https://doi.org/10.3390/rs15092387

Smith, S. E., Haferkamp, M. R., & Voigt, P. W. (2004). Gramas. In L. E. Moser, B. L. Burson, & L. E. Sollenberger (Eds.), *Warm-Season (C4) Grasses* (Vol. 45). American Society of Agronomy, Inc., Crop Science Society of America, Inc., Soil Science Society of America, Inc.

Sticpewich, H. (2022). *Microhydrology of a Periodically-Patterned Arid Grassland: Surface Water Dynamics, Infiltration, and Soil Water Accumulation in a Simulated Rainfall Experiment* [Colorado College]. https://digitalcc.coloradocollege.edu/record/4456?ln=en&p=haidee+sticpewich&v=pdf

Tongway, D. J., & Ludwig, J. A. (1990). Vegetation and soil patterning in semi-arid mulga lands of Eastern Australia. *Australian Journal of Ecology, 15*, 23–34.

Tongway, D. J., & Ludwig, J. A. (2001). Theories on the Origins, Maintenance, Dynamics, and Functioning of Banded Landscapes. In D. J. Tongway, C. Valentin, & J. Seghieri (Eds.), *Banded Vegetation Patterning in Arid and Semiarid Environments: Ecological Processes and Consequences for Management* (Vol. 149, pp. 20–31). Springer.

USDA NRCS Plant Materials Program. (2006). *Plant Fact Sheet: Blue Grama*. US Department of Agriculture Natural Resources Conservation Service.

Valentin, C., & d'Herbès, J. M. (1999). Niger tiger bush as a natural water harvesting system. *CATENA, 37*(1), 231–256. https://doi.org/10.1016/S0341-8162(98)00061-7

Valentin, C., d'Herbès, J. M., & Poesen, J. (1999). Soil and water components of banded vegetation patterns. *CATENA, 37*(1), 1–24. https://doi.org/10.1016/S0341-8162(99)00053-3

van de Koppel, J., & Rietkerk, M. (2004). Spatial Interactions and Resilience in Arid Ecosystems. *The American Naturalist, 163*(1), 113–121. https://doi.org/10.1086/380571

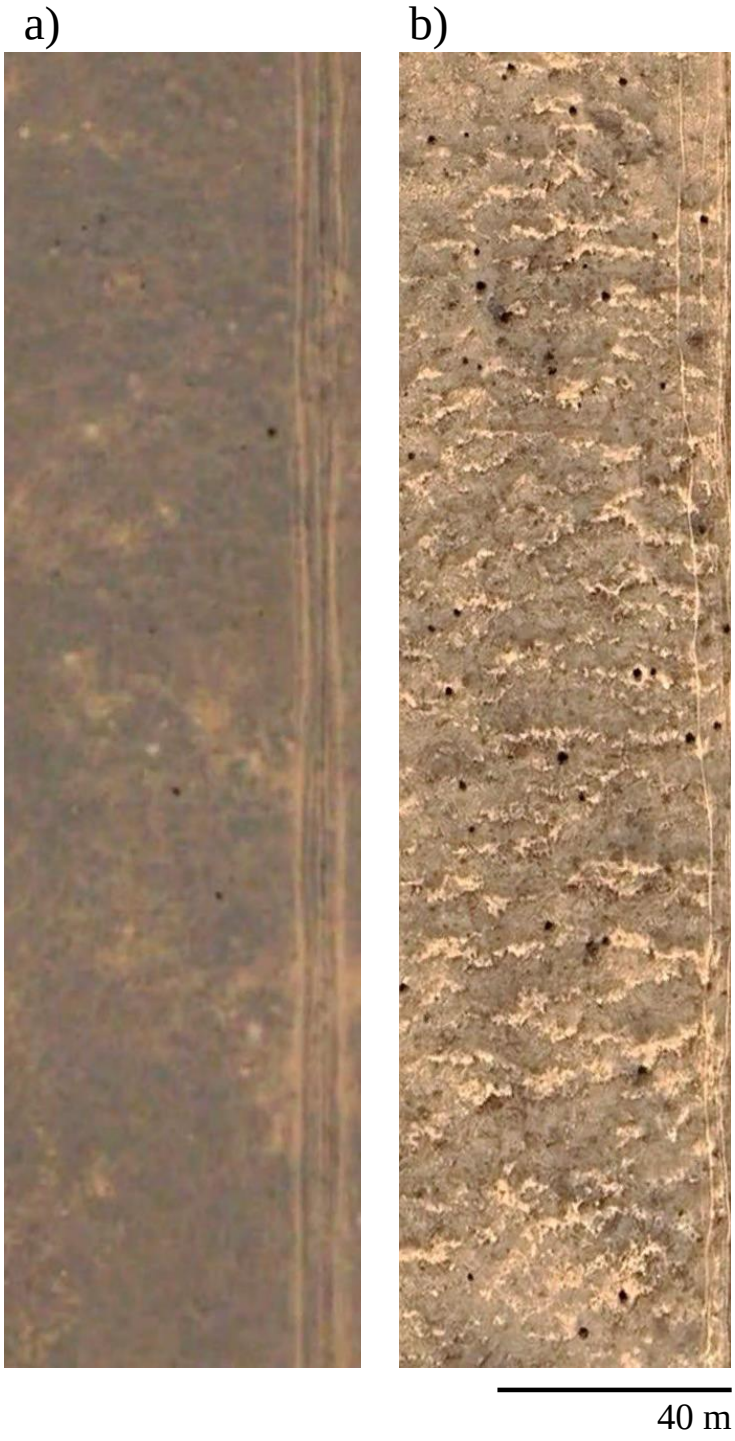

Figure 1: Aerial imagery of Chico Basin Ranch study site in (a) 2003 and (b) 2023, obtained from Google Earth.

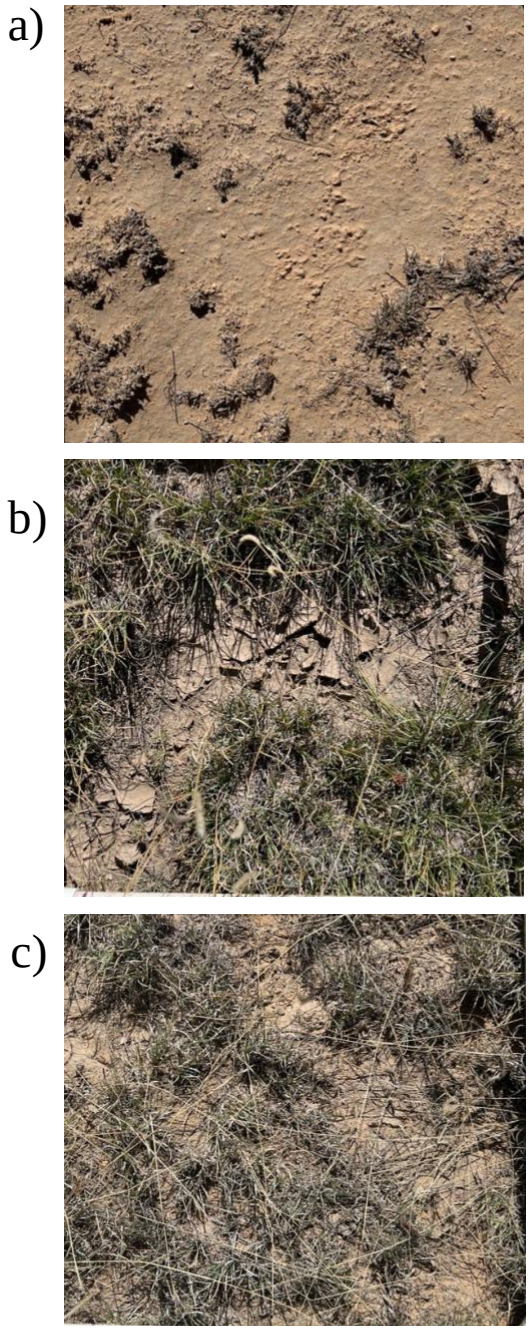

Figure 2: Representative (a) intergrove and (b) interstitial pool in the grove and (c) early senescing grass in the downslope grove. Photos approximately 50 cm by 50 cm.

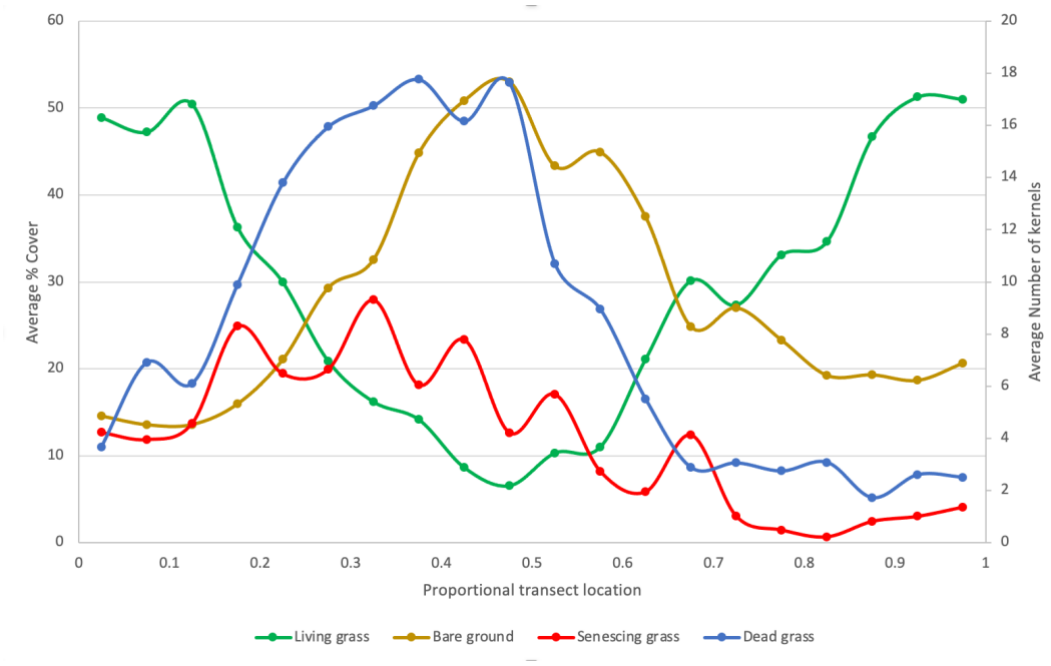

Figure 3: Aggregate plot of average land cover type plotted by a normalized transect distance. Average living grass and bare ground are plotted on the left y-axis as percent coverage, and dead grass and senescing grass are plotted on the right y-axis as number of kernels.

a)

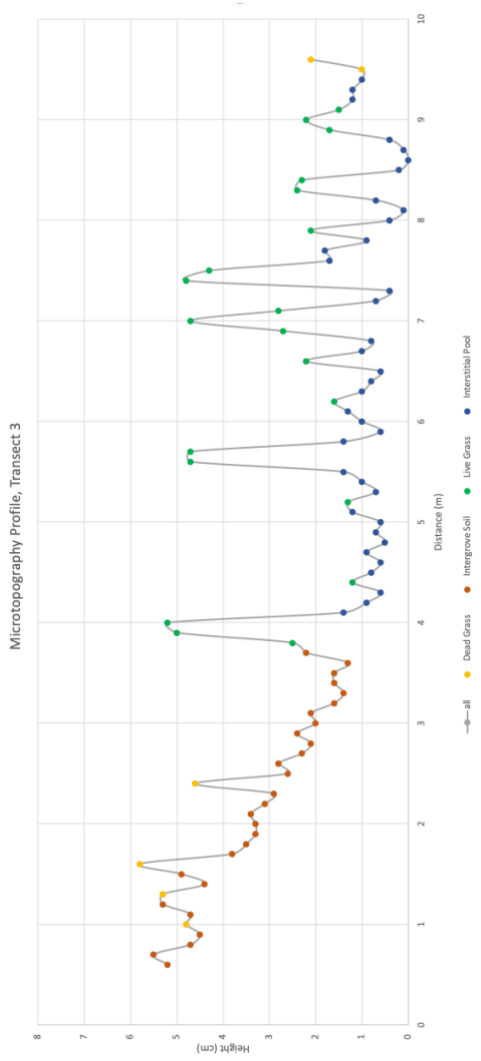

b)

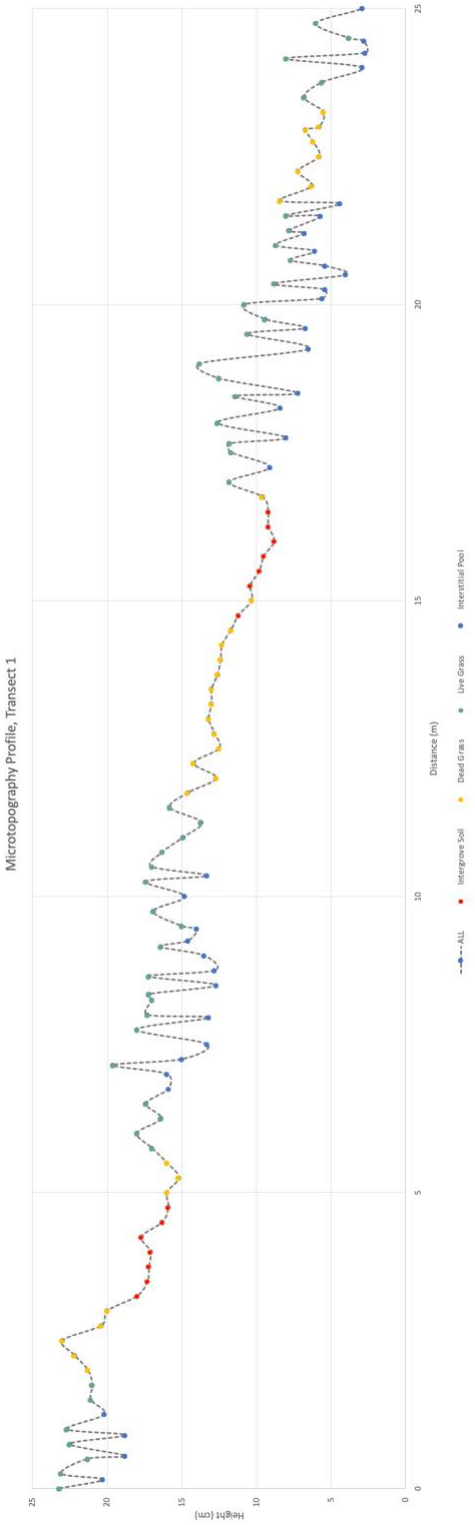

Figure 4: Microtopographic profiles of (a) a transect of one intergrove-grove unit and (b) a transect of two intergrove-grove units.

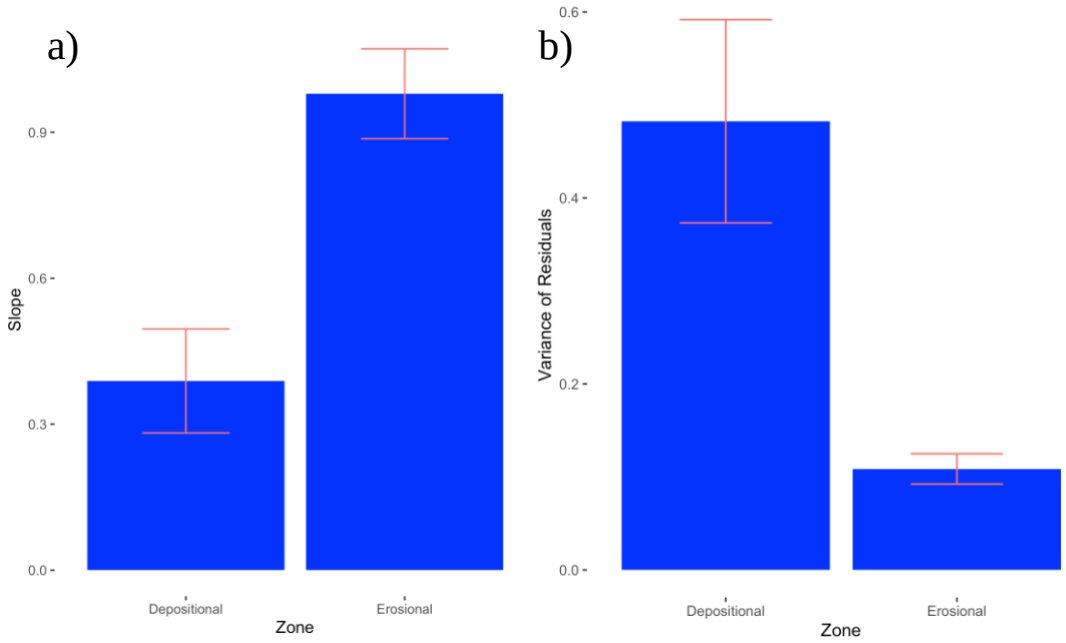

Figure 5: Microtopographic profile analyses of (a) mean slope (cm/m) by zone and (b) mean variance of residuals (roughness) by zone.

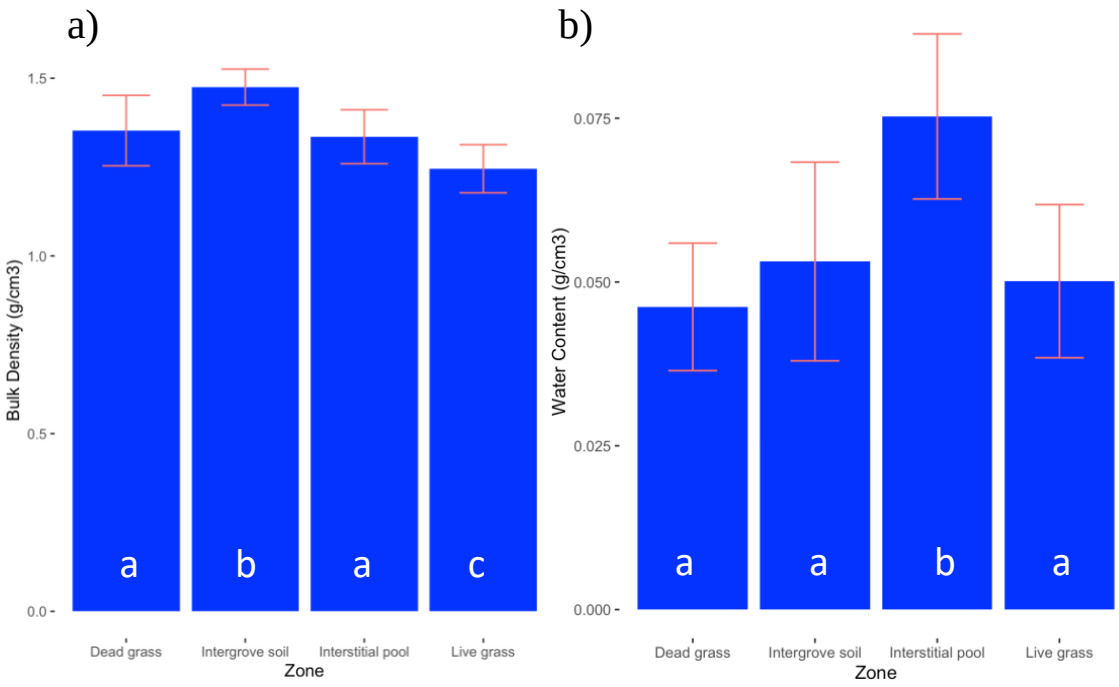

Figure 6: Soil core analyses of (a) mean bulk density (g) by zone and (b) mean water content (g) by zone.

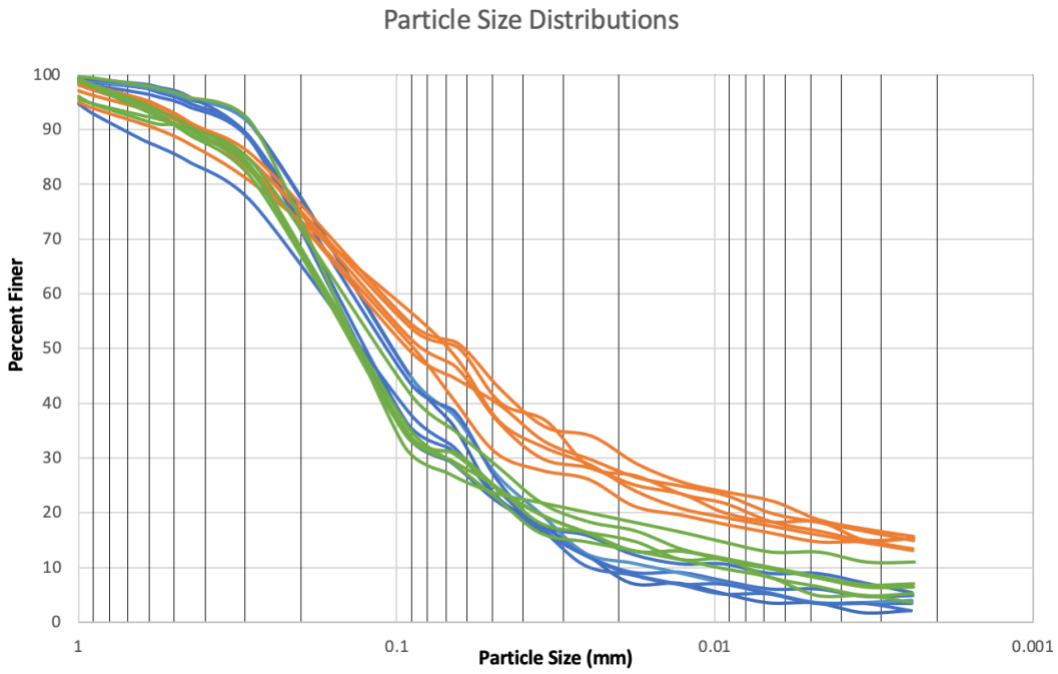

Figure 7: Particle size distributions of intergrove dust (blue), intergrove crust (green), and depositional pool crust (orange). For a given particle size, the value on the y axis corresponds to the percent of particles smaller than that size threshold.

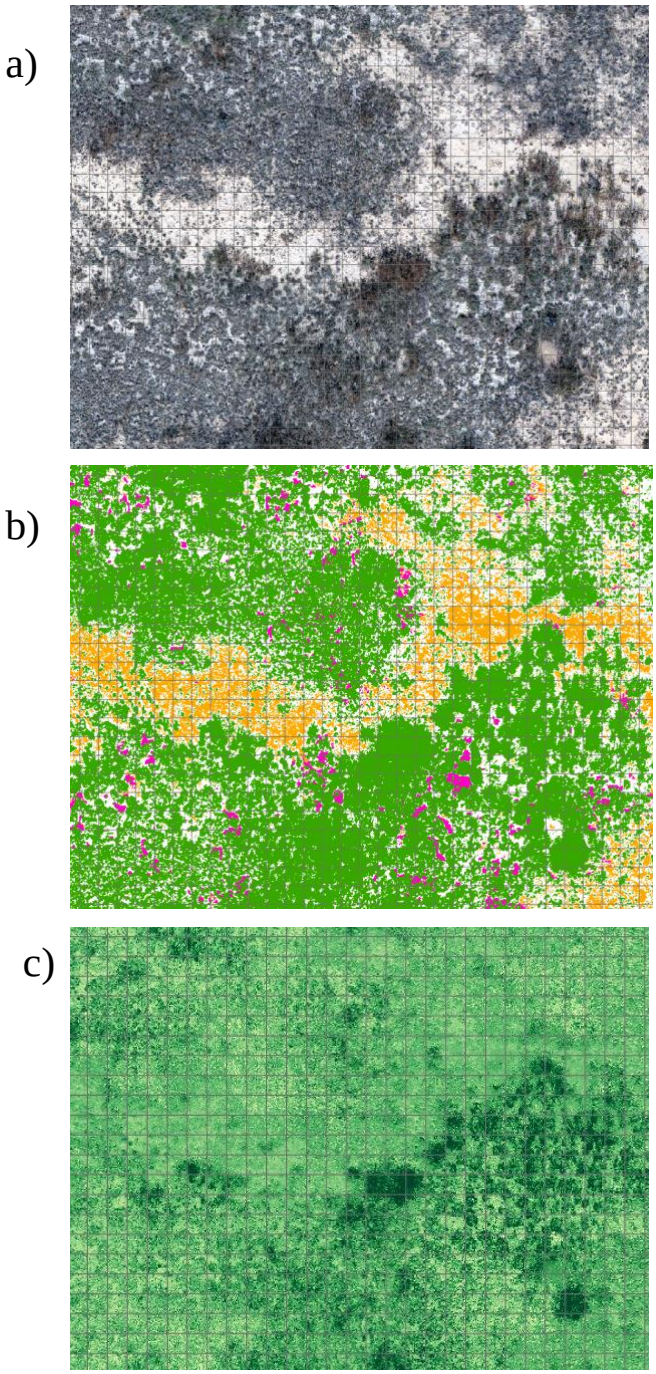

Figure 8: Representative band as captured by UAV visualized as (a) the raw orthomosaic, (b) the improved surface classification into vegetation (green), intergrove soil (orange), and depositional pools (pink), and (c) NDVI from low to high in light blue/green to pink/red. Grid used for correlations and spatial regressions is at a 0.5 m scale.

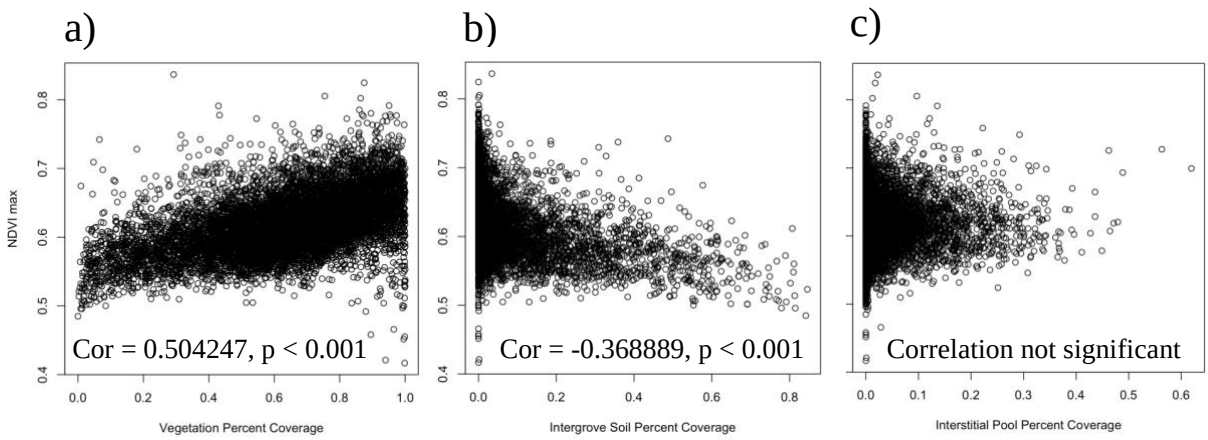

Figure 9: Plots of NDVI max by (a) vegetation percent coverage, (b) intergrove soil percent coverage, and (c) interstitial pool percent coverage with displayed correlation coefficients.

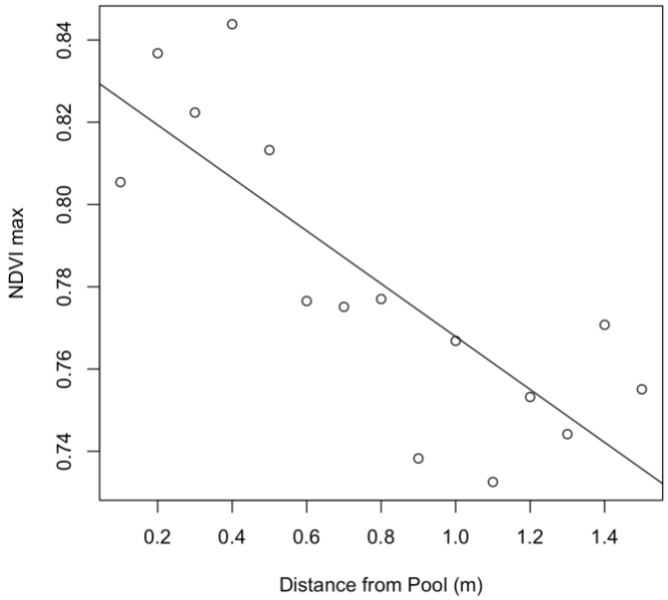

Figure 10: NDVI max by successive nested buffers increasing in distance

Table 1: Spatial Regression Results

	Dependent Variable: NDVI max			
	OLS (non-spatial)	SEM	SLX	SLM
Vegetation Density	0.098***	0.099***	0.099***	0.091***
	(0.002)	(0.002)	(0.002)	(0.002)
Interstitial Pool Cover	0.042***	0.044***	0.045***	0.038***
	(0.007)	(0.007)	(0.007)	(0.006)
Lagged Vegetation Density			-0.002	
			(0.003)	
Lagged Interstitial Pool Cover			-0.021	
			(0.015)	
Constant	0.556***	0.555***	0.557***	0.386***
	(0.001)	(0.001)	(0.002)	(0.009)
Observations	9,781	9,781	9,781	9,781
R2	0.257		0.258	
Adjusted R2	0.257		0.257	
Log Likelihood		18,524.740		18,474.380
sigma2		0.001		0.001
Akaike Inf. Crit.		-37,039.490		-36,938.770
Residual Std. Error	0.037 (df = 9778)		0.037 (df = 9776)	
F Statistic	1,694.929*** (df = 2; 9778)		847.981*** (df = 4; 9776)	
Wald Test (df = 1)		461.426***		370.458***
LR Test (df = 1)		471.501***		370.785***
Note:				*p<0.1; **p<0.05; ***p<0.01